Proceedings of the 25th International Conference on
Port and Ocean Engineering under Arctic Conditions
June 9-13, 2019, Delft, The Netherlands

Model assumptions in rig icing and their implications

Arne Bøckmann[1], Olga Shipilova[1], Ole-Christian Ekeberg[1]
[1] DNV GL, Høvik, Norway

ABSTRACT

Marine icing simulations include a variety of models for heat transfer, water film motion, phase change and sea spray. Many of these are coupled and non-linear, and some – such as the sea spray models – are associated with a high degree of uncertainty. We analyze and discuss the implications of a variety of model assumptions in the analysis of a well-known case of icing on a rig. It is shown that parameters which are often not given much thought may exert a large influence on the ice accretion.

KEY WORDS

Marine icing; Numerical Simulation; Modelling; Sensitivity; RigSpray JIP

NOMENCLATURE

Greek letters

η	Water film thickness
ρ	Density
χ	Length coordinate in normal direction
ν	Kinematic viscosity of water
α	Interfacial distribution coefficient
σ	Stefan-Boltzmann constant
ε	Emissivity
θ	Angle between vertical and surface
∇_s	Surface gradient operator

Subscripts

f	Freezing
v	Vaporization
s	Water film surface
ac	Ice accretion
int	Water/ice Interface
sea	Sea
a	Air
i	Pure ice
w	Water film
sp	Spray
wc	Whitecap
fs	Fluid-structure

Latin letters

r	Relative humidity
b	Ice thickness
k	Thermal conductivity
T	Temperature
S	Salinity
F	Flux
L	Latent heat
c	Specific heat capacity at constant pressure
g	Gravity vector
n	Surface unit normal vector
$\tilde{\boldsymbol{u}}$	Depth-averaged velocity vector in fluid film
Q_d	Sensible heat flux
Q_e	Evaporative heat flux
Q_r	Radiative heat flux
Q_c	Convective heat flux

Other/exceptions

e_s	Saturation pressure
Le	Lewis number
H_s	Significant wave height

INTRODUCTION

Marine icing has been known as a problem for a long time (Shellard 1974), but research and documentation started to pick up momentum in the second half of the 1900s. Early icing predictions were based on nomograms, typically with wind speed, air temperature and sea temperature as input parameters (Sawada 1962; Mertins 1968; Lundqvist & Uding 1977). The nomograms were later extended to analytic expressions based on physical considerations (Overland, Pease & Preisendorfer 1986) and more involved methods based on iterative procedures (Stallabrass 1980). As computers became sufficiently powerful, the physical equations governing macroscopic freezing were solved numerically in space and time (Horjen & Vefsnmo 1985; Horjen & Vefsnmo 1987). The numerical simulations have in later times been modernized, but the essentials remain the same. The icing rate can be computed locally by assuming a supercooled saline fluid film and solving the transport equations of water and salt subject to freezing under various heat transfer mechanisms and spray conditions. The environmental driving factors are typically air temperature and humidity, sea temperature, winds speed and direction and wave height. There are however several assumptions which need to be made to close the icing model. These include, but are not limited to: spray flux, temperature, salinity and collision efficiency, wind profile, vessel motions, the characteristics of wave washing and the roughness of the surface at which heat transport to the environment takes place. The present paper uses a well-known case of icing on the drilling rig Ocean Bounty to address the effect of some of these assumptions, as implemented in the software code developed in the RigSpray Joint Industry Project.

ICING MODEL

The RigSpray icing model assumes that the icing is driven by heat transport through a supercooled saline water film covering the structure. The model solves conservation equations for water, salt and ice, coupled with heat transfer equations on the film surface, and an equation describing freezing on the film/ice interface. The transport equations for film motion and salt (Eqs. (1)-(3)) are solved on a general unstructured surface mesh using a vertex centered finite volume discretization method (Ham, Mattsson & Iaccarino 2006), and the heat transport equations are generally nonlinear, requiring iterations between Eqs. (4) and (5) to find the film surface temperature T_s. The icing over a 3-hour metocean state is approximated by estimating the icing rate from a much shorter time series (typically two spray periods) and extrapolating the icing rate to the rest of the metocean state. The model is otherwise similar to that of (Kulyakhtin & Tsarau 2014). The main model assumptions are illustrated in Figure 1. It is assumed that the water and ice at the icing interface $\chi = b$ are in thermal equilibrium and thus, the temperature here is the freezing temperature T_f, which is a function of the film salinity. It is further assumed that all latent heat from freezing is transferred from the icing interface and into the film – not into the ice accretion, which is assumed perfectly insulated. The water film is assumed to almost instantly adjust its temperature profile to the end-point temperatures T_f and T_s due to its thinness, such that a linear temperature profile is an adequate assumption (Eq. (4)). The ice is assumed to be spongy, which means that it contains entrapped pockets of unfrozen water. The interfacial distribution coefficient $\alpha \equiv \frac{S_{ac}}{S_w}$ which determines the water/ice ratio is given by Eq. (6). The heat transfer coefficients are obtained by CFD simulations at a fixed wind velocity and fixed directions. They are then extended to any direction and any wind velocity by interpolating between directions, and extrapolating to the desired wind velocity by Eq. (11). The exponent in Eq. (11) is an approximation found from an empirical investigation, and is inspired by the form of empirical expressions for heat transfer on cylinders.

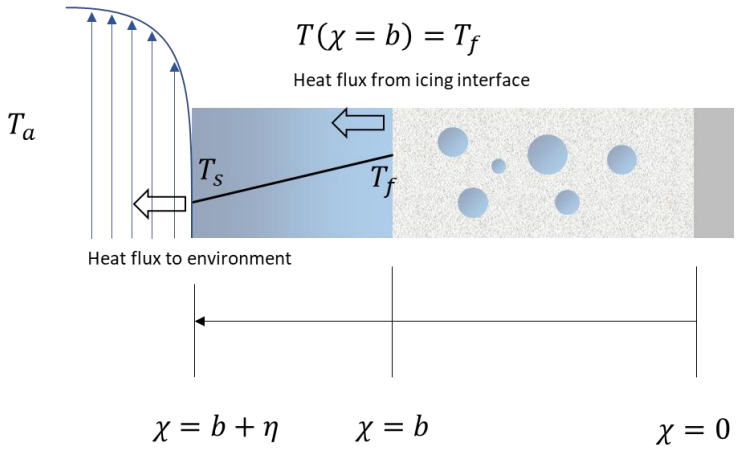

Figure 1. Illustration of the icing model. From right to left: substrate, ice accretion, water film and environment (ambient conditions).

While the full model is too comprehensive to be described completely in the present work, the most important conservation equations and constitutive relations are given in Table 1, with nomenclature given at the beginning of the article.

Table 1. Equations of the icing model.

Model	Comment	Equation	Eq. no.
Mass conservation equations for brine and salt in water film		$\rho_w\left(\frac{\partial \eta}{\partial t} + \nabla_s \cdot (\tilde{\boldsymbol{u}}\eta)\right) = -\rho_{ac}\frac{db}{dt} - \frac{Q_e}{L_v} + F_{sp}$	(1)
		$\rho_w\left(\frac{\partial (\eta S_w)}{\partial t} + \nabla_s \cdot (\tilde{\boldsymbol{u}}\eta S_w)\right) = -\rho_{ac}S_{ac}\frac{db}{dt} + F_{sp}S_{sp}$	(2)
		$\tilde{\boldsymbol{u}} = \frac{\eta^2}{3\nu}((\boldsymbol{g} - (\boldsymbol{g}\cdot\boldsymbol{n})\boldsymbol{n}) + (\boldsymbol{g}\cdot\boldsymbol{n})\nabla_s\eta)$	(3)
Heat balance between film surface and environment		$Q_d + Q_r + Q_c + Q_e = -\frac{k_w}{\eta}\left(T_s - T_f(S_w)\right).$	(4)
Heat fluxes on film surface	Emissivities from (Li, Jiang & Coimbra 2017; Maykut & Church 1973). The cloud fraction C is set to a constant value of 0.8.	$Q_d = c_w F_{sp}(T_f - T_{sp})$ $Q_r = \sigma(\varepsilon_s T_s^4 - \frac{\pi - \theta}{\pi}\varepsilon_a T_a^4 - \frac{\theta}{\pi}\varepsilon_{sea}T_{sea}^4)$ $Q_c = h(T_s - T_a)$ $Q_e = \frac{\xi L_v}{pc_a}Le^{-0.63}h\left(e_s(T_s) - re_s(T_a)\right)$ $\varepsilon_a = (1 + 0.22C^{2.75}) \times \left(0.618 + 0.0056\sqrt{re_s(T_a)}\right),$ $\varepsilon_s = \varepsilon_{sea} = 1$	(5)

Model	Comment	Equation	Eq. no.
Heat balance between film and latent heat released by freezing	α is based on data from (Makkonen 2010)	$-\frac{k_w}{\eta}\left(T_s - T_f(S_w)\right) = \rho_{int} L_f (1-\alpha)\frac{db}{dt}$ $\alpha = 0.3 - \min\left(0, 1.77\times 10^{-2}\left(T_{sp} - T_{sp,f}\right)\right)$	(6)
Mass and salt balance between ice accretion and water film		$\frac{d\rho_{ac}}{dt} = \frac{\rho_{int} - \rho_{ac}}{b}\frac{db}{dt}$	(7)
		$\frac{\partial(b\rho_{ac}S_{ac})}{\partial t} = \rho_{int} S_{int}\frac{db}{dt}$	(8)
Salinity and density on freezing/melting ice on interface between ice accretion and water film		$S_{int} = \begin{cases} \alpha S_w & \text{if } \frac{db}{dt} > 0 \\ S_{ac} & \text{if } \frac{db}{dt} < 0 \end{cases}$	(9)
		$\rho_{int} = \begin{cases} \left(\frac{\alpha}{\rho_w} + \frac{1-\alpha}{\rho_i}\right)^{-1} & \text{if } \frac{db}{dt} > 0 \\ \rho_{ac} & \text{if } \frac{db}{dt} < 0 \end{cases}$	(10)
Extrapolation of heat transfer coefficient *h* at wind velocity U_0 to wind velocity U		$h(U,x) \approx \left(\frac{U}{U_0}\right)^p h(U_0,x)$ $p = 0.7$	(11)
Wave washing (ice under R_M is removed) (Mitten 1994)	k is a characteristic wave number (taken as $\frac{\pi}{10H_s}$ in the present case) and L is a characteristic length scale.	$R_M = \begin{cases} 0.5H_s(2.0589 + 2.3292kL - 1.3194(kL)^2) - 0.5H_s & kL < 0.9 \\ H_s & kL > 0.9 \end{cases}$	(12)
Whitecap spray (Jones & Andreas 2012)	$U_{10} < 19\ m/s$: $F_{sp,wc}(z) = \int_5^{100} \frac{4}{3}\pi(10^{-6}\times r_{80})^3 \rho_w \frac{7\times 10^4 U_{10}^3}{r_{80}} \exp\left(-\frac{1}{2}\left[\frac{\log\left(\frac{r_{80}}{0.3}\right)}{\log(2.8)}\right]^2\right) z^{\frac{-V_g(r_{80})}{0.4u^*(U_{10})}} dr_{80}$ $U_{10} \geq 19\ m/s$: $F_{sp,wc}(z) = \int_5^{200} \frac{4}{3}\pi(10^{-6}\times r_{80})^3 \rho_w \frac{30 U_{10}^5}{r_{80}} \exp\left(-\frac{1}{2}\left[\frac{\log\left(\frac{r_{80}}{0.3}\right)}{\log(4)}\right]^2\right)\left(\frac{2z}{H_s}\right)^{\frac{-V_g(r_{80})}{0.4u^*(U_{10})}} dr_{80}$ where r_{80} is the equilibrium radius for droplets at 80% relative humidity, and u^* is the friction velocity.		(13)

Model	Comment	Equation	Eq. no.
Fluid-structure interaction spray (Horjen & Vefsnmo 1985)	Modelled as pulses of period τ_{sp}=20s, and duration τ_{dur} = 2s.	$F_{sp,fs}(z) = \frac{M_{HV} U_{10} \tau_{sp}}{\tau_{dur}} \frac{1-\left(1-10^{-2} U_{10}\right) \exp\left(-\left(\frac{4z_{HV}+2}{9}\right)^2\right)}{\exp\left(k_{HV} U_{10}^{2/3} z_{HV}^2\right)}$	(14)

CASE STUDY

To check the effect of different modelling choices, we use data from the icing storms endured by the drilling rig Ocean Bounty near Kamishak Bay in Lower Cook Inlet, Alaska in the winter 1979-1980 (Nauman 1984; Jones & Andreas 2009). The most severe storm produced an ice load of around 508 metric tons.

The period between November 19th 1979 and March 3rd 1980 is simulated. The time history of relevant metocean parameters is given in (Jones & Andreas 2009). This list is however incomplete; it lacks data for several periods, and it only accounts for periods with temperatures near or below 0ºC for at least a portion of the day. As a result, missing data has been estimated by linear interpolation between the closest data points, where only one or a few of the environmental parameters are missing. For longer periods where all environmental parameters are missing, it has been assumed that all ice has been removed. Relative humidity has been computed from the air temperature and dew point temperature. These do not always coexist in the metocean time series, leading to interpolation that produces higher relative humidity than 100% for some periods. The relative humidity has thus been capped at 100%. Wind speed is corrected to 10 m above SWL using the anemometer height on Ocean Bounty (84 m above SWL) and the height dependency of the Frøya wind profile (DNVGL-RP-C205 August 2017):

$$U_{84} \approx U_{10}\left(1 + 0.0573\sqrt{1 + 0.148 U_{10}} \log\left(\frac{84}{10}\right)\right) \quad (15)$$

with U in [m/s].

As an approximative visualization of the expected icing severity, the Overland icing predictor (Overland, Pease & Preisendorfer 1986; Overland 1990) applied to the metocean time series has been plotted in Figure 2.

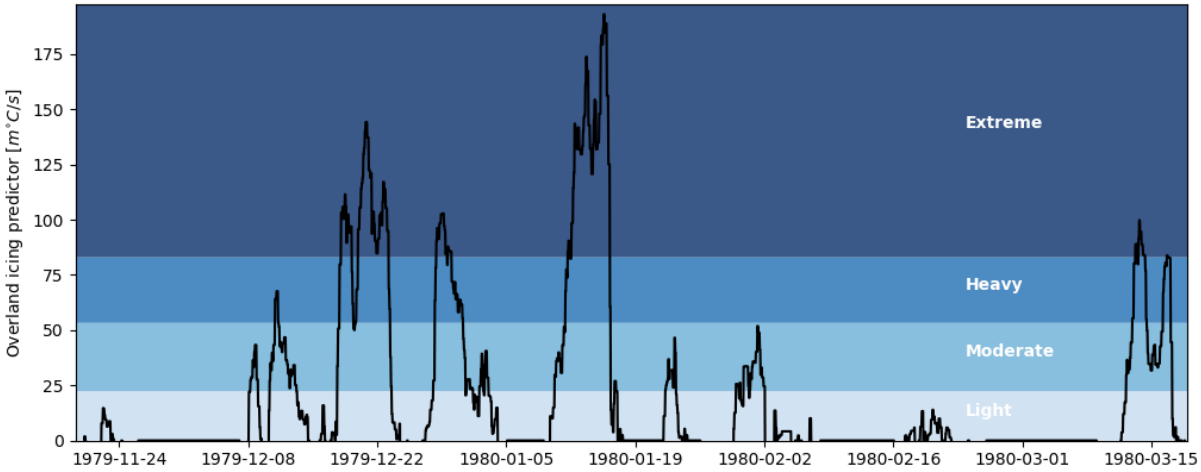

Figure 2. The Overland icing predictor for the metocean data used in the case study.

The vessel orientation is not given, but the 0-degree heading is assumed to be aligned with the x-axis; see Figure 3. This should not matter much in the icing analysis, since the main contribution is icing on the cylindrical columns. The vessel geometry is only crudely sketched in (Nauman 1984). Based on this and photos found of the rig, the estimated vertical column positions and diameters are given in Table 2. Bottom Of Steel is located 15.24 m above MWL, at which the deck has been modelled as a solid plate of thickness 2.43 m.

CFD simulations to determine the heat transfer coefficients have been performed using a transient finite volume solver with an unstructured mesh, see Figure 3. The wind velocity has been set to a uniform value (U_0 in Eq. (11)) of 30 m/s, and 8 discrete wind directions are simulated, using increments of 45 degrees. The domain is a cylinder of diameter 1 km and height 400 m. The floor in the CFD domain corresponds to the Still Water Level (SWL), and has a free-slip boundary condition assigned to it. To maintain ambient turbulence in the absence of a boundary layer above the ocean surface, volumetric source terms for turbulent energy have been added in the k-ω turbulence model. The rig surface is assumed to be smooth, with a no-slip boundary condition. To extrapolate the heat transfer coefficient to other wind speeds, U in Eq. (11) is chosen as the velocity 10 m above SWL.

Table 2. Estimated column layout for Ocean Bounty.

Horizontal coordinate (x,y) [m]	Diameter [m]
(40.5, 14)	7.5
(40.5, -14)	7.5
(-40.5, 14)	7.5
(-40.5, -14)	7.5
(14, 40.5)	7.5
(-14, 40.5)	7.5
(14, -40.5)	7.5
(-14, -40.5)	7.5
(14, 14)	3.0
(-14, 14)	3.0
(14, -14)	3.0
(-14, -14)	3.0

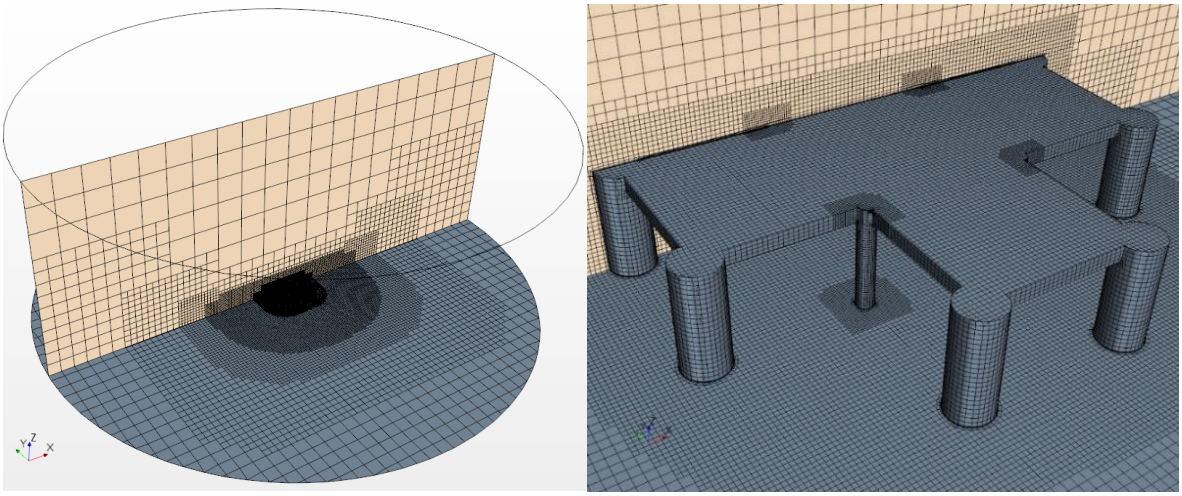

Figure 3. CFD domain and mesh. Left: Cylindrical domain, right: close-up near structure.

The physics and modelling choices we wish to study are:

- The inclusion of whitecap spray
- Assumptions on whitecap spray salinity
- Assumptions on lee-side spray flux
- Assumptions on droplet collision efficiency (the fraction of spray in the undisturbed air which impacts on the surface)
- The effect of evaporative mass transfer
- The contribution of wave-washing (the melting of ice due to wave run-up)
- Relative contributions of different heat transfer mechanisms

For this purpose, we define a base case and variation cases, with properties as given in Table 3.

Table 3. Case definitions.

Case	Properties
Base case (BC)	• Structure interaction spray (Horjen & Vefsnmo 1985) included, at a temperature and salinity equal to the sea surface temperature and salinity. • White-cap spray flux based on a relative humidity of 80% (Jones & Andreas 2012) included. Assumes a spray temperature equal to the air temperature, and a salinity equal to the sea surface salinity. • Spray collision efficiency is 100%, as compared to the undisturbed fluxes in the spray models. • No spray on lee side. • Convective, evaporative, sensible and radiative heat transfer included. • Evaporative mass transfer included. • Wave washing included, characteristic length scale set to largest column diameter.
Variation case 1 (VC1)	Whitecap spray disabled.
Variation case 2 (VC2)	Whitecap spray salinity set equal to 8 times the sea surface salinity. (Andreas 1990). This is based on the equilibrium droplet radius at 80% relative humidity (r_{80}), which due to evaporation is half the radius at droplet generation. The volume of these droplets is thus 1/8 of the original volume, increasing the salinity compared to that at generation by a factor of 8.

Case	Properties
Variation case 3a (VC3a)	Variation case 2 + Collision efficiency (Finstad, Lozowski & Gates 1988) included in expression for whitecap spray flux. Based on the droplet equilibrium radius at 80% relative humidity – r_{80} – and the diameter of the largest columns.
Variation case 3b (VC3b)	As Variation case 3a, but with collision efficiency based on collisions with cylinders of diameter 5 cm.
Variation case 4 (VC4)	Lee side spray flux modeled by $F = F_{sp}\max(cos\ \beta, 0.06)$ where F is the spray flux hitting the surface, F_{sp} is the undisturbed spray flux normal to the wind velocity vector, and β is the angle between an inward pointing surface normal and the wind velocity vector. This intends to approximate a roughly 10% spray flux contribution from the lee side, see (Jørgensen 1984).
Variation case 5 (VC5)	Evaporative mass transfer disabled ($\frac{Q_e}{L_v}$ in Eq.(1)).
Variation case 6 (VC6)	Variation case 4 + 5.
Variation case 7 (VC7)	Wave washing disabled.

RESULTS AND DISCUSSION

The base case (BC), which reflects choices that are thought to be slightly on the conservative side and suitable for an engineering analysis, predicts the maximum total ice load on Ocean Bounty to be 548 metric tons; about 8% higher than the 508 metric tons reported in (Nauman 1984). While this is considered a good match, we shall see that the value is highly dependent on model assumptions.

The maximum ice mass in each case is tabulated in Table 4. The time history of the base case total ice mass is plotted Figure 4, together with the corresponding contributions of different heat transfer mechanisms. We see that in periods of severe icing, convective mass transfer is by far the dominant mechanism, with radiative heat transfer increasing in importance for periods of light icing or melting. The time histories of all cases are compared in Figure 5.

The data shows that one of the most important mechanisms that affect the ice load is wave washing (VC7). The wave washing model estimates the run-up height. All ice in the run-up zone is assumed to melt. Since most of the ice accumulates near the ocean surface, run-up can remove a significant fraction of the total ice load. The model deviates from reality in two important aspects. Firstly, wave washing is not likely to manifest as an abrupt boundary under which no ice exists, but as a gradual transition. Secondly, the relative motions of the vessel are not accounted for. A vessel with motion out of phase with the waves will clearly experience more wave washing (and probably spray) than a vessel which follows the wave motion.

From the case without whitecap spray, we see that whitecap spray accounts for more than 40% of the maximum ice load. This is however based on the assumption that whitecap spray has the same salinity as the sea water. It is observed in (Andreas 1990) that the equilibrium radius at 80% relative humidity is half of the radius at droplet generation due to evaporation. This means that the droplet salinity is 8 times higher than that of the sea surface. The exact fraction of whitecap spray that has reached its equilibrium radius is not known, and the salinity is likely a conservative guess. The results show that whitecap spray may contribute negatively to the total ice load due to its high salinity (VC2) by lowering the freezing

temperature in the water film. However, inclusion of collision efficiency for whitecap spray reduces its influence significantly, since the large structure and very small droplets cause most of the spray to be deflected around the structure (VC3a). Assuming that the spray collides with small-scale geometry (such as piping, rails etc.) instead by setting the structural diameter to 5 cm in the expression for collision efficiency (VC3b) increases the influence of whitecap spray from virtually nothing (VC3a), but still yields a negative contribution to the total ice load due to the elevated salinity.

Assuming some spray flux also on the lee side of the structure vastly increases the area where heat transfer can produce ice (VC4). The water film here is thinner however, and icing may thus stop earlier, since the salinity of the film is increased more easily by freezing and evaporation. When neglecting evaporative mass transfer (VC5), the maximum ice mass increases by 14%, compared to the base case. When including lee side spray, the increase in maximum ice mass from neglecting evaporative mass transfer is 22% (VC6), implying that evaporative mass transfer exerts a higher effect on icing under thin films, as expected.

The typical computation time on a laptop was 15 minutes per case.

Table 4. Maximum ice mass recorded during simulation period.

Case	Maximum ice mass [metric tons]
BC	548
VC1	313
VC2	244
VC3a	313
VC3b	259
VC4	627
VC5	628
VC6	771
VC7	1946

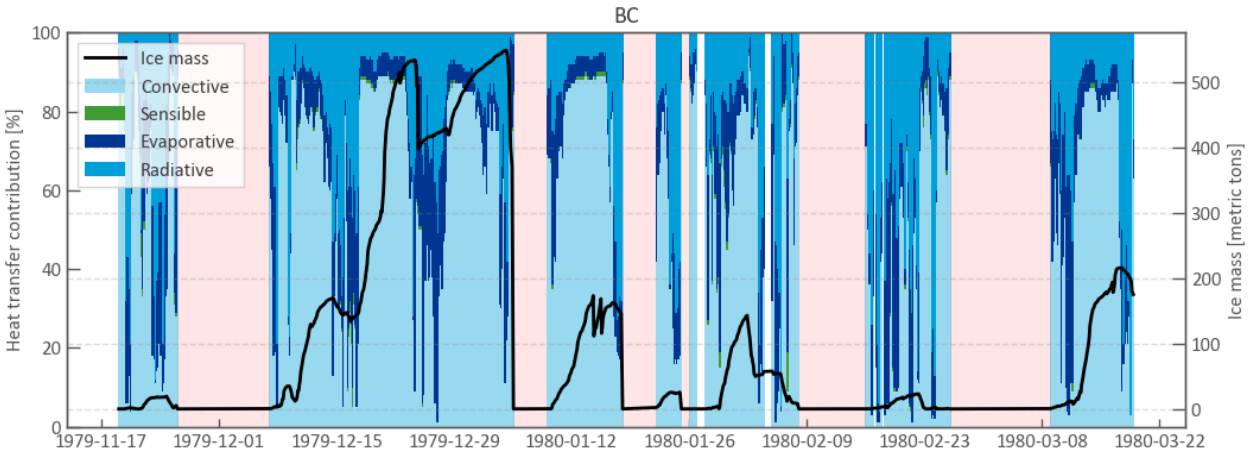

Figure 4. Wetted area-averaged relative magnitude of heat transfer mechanisms for base case.

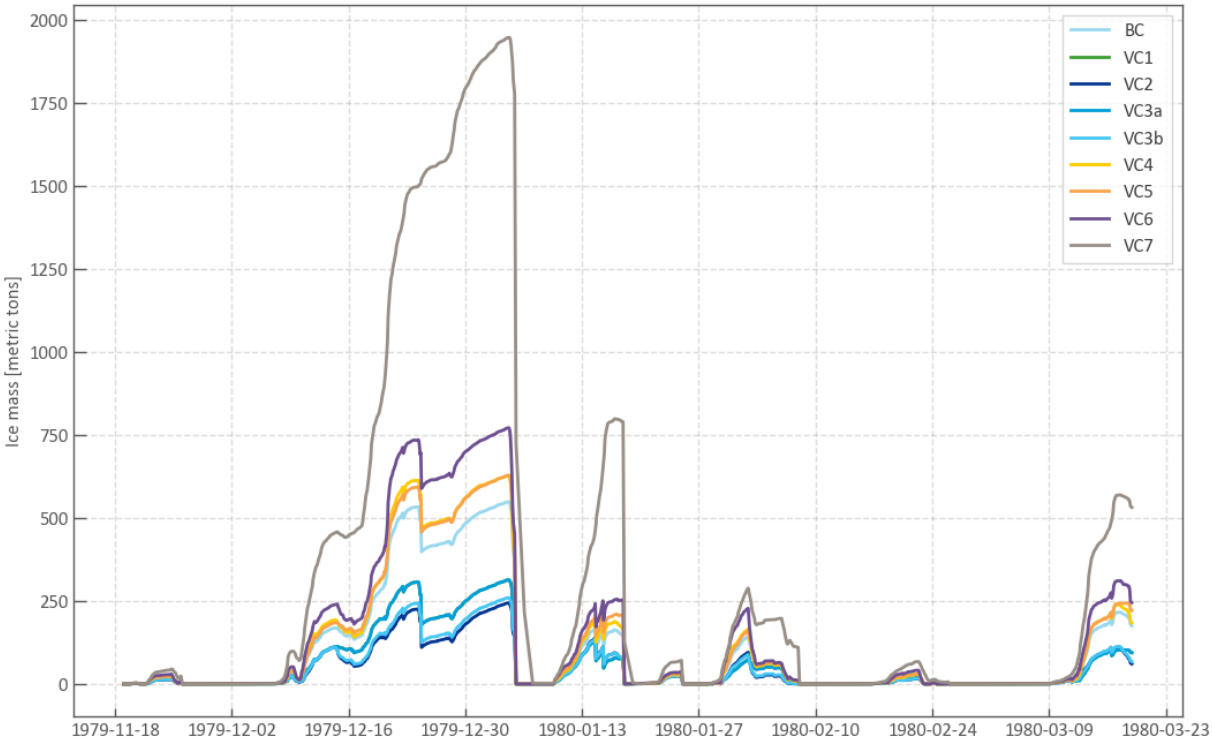

Figure 5. Time history of ice mass for all cases. Note that the curve VC1 is almost entirely hidden behind VC3a.

CONCLUSIONS

It is shown that relatively innocuous modelling choices can significantly affect the total predicted ice mass under realistic environmental conditions, and in particular, the combined effect of different modelling choices can be large. Since the icing model is non-linear, the effect of changing one model parameter cannot easily be generalized but depends on the environmental conditions and the other model parameters. In our simulations of a well-known case of icing, the reported ice mass could be overestimated by around 280% or underestimated by around 50% depending on the modelling choices. For some of these choices, there is either insufficient data to make an informed choice, or the real phenomenon is so exceedingly complex that the value of simplified models may be questionable.

The strongest effect on the ice mass was exerted by the wave washing model, which removes all ice beneath the run-up height. The high sensitivity to this model is caused by the fact that the cut-off limit for ice removal typically coincides with the location of the highest ice thickness.

The equations presented here include only a subset of the constitutive relations needed to close the icing model, making the total icing model a large collection of sub-models – some associated with a high degree of uncertainty. Despite the uncertainty, the base case settings – which were not tuned to produce the desired result - predicted the real ice mass to 548 metric tons, which is 8% higher than the real case. 548 tons is also the median of all the tested cases, suggesting that good predictions may be possible, but that a high degree of caution should be exercised when performing icing analyses.

ACKNOWLEDGEMENTS

The present work is part of the RigSpray Joint Industry Project. RigSpray aims to improve the prediction of marine icing. It is funded by The Norwegian Research Council with Grant No. 256435 through the PETROMAKS2 programme, and participants SINTEF, Equinor Energy, OMV (Norge), Vår Energi, Aker BP and Lundin Norway.

REFERENCES

Andreas, EL 1990, 'Time constants for the evolution of sea spray droplets', *Tellus B: Chemical and Physical Meteorology*, vol 42, no. 5, pp. 481-497.

DNVGL-RP-C205 August 2017, 'Environmental conditions and environmental loads'.

Finstad, KJ, Lozowski, EP & Gates, EM 1988, 'A computational investigation of water droplet trajectories', *Submitted to Journal of Atmospheric and Oceanic Technology*, vol 5, pp. 160-170.

Ham, F, Mattsson, K & Iaccarino, G 2006, 'Accurate and stable finite volume operators for unstructured flow solvers', *Annual Research Briefs, Center for Turbulence Research, NASA Ames/Stanford University*, pp. 243-261.

Horjen, I & Vefsnmo, S 1985, 'A kinematic and thermodynamic analysis of sea spray (in Norwegian)', *Offshore Icing - Phase II, Norwegian Hydrotechnical Laboratory (NHL), Report STF60 F85014*.

Horjen, I & Vefsnmo, S 1985, 'Computer modelling of sea spray icing on marine structures', Proceedings of Symposium on Automation for Safety in Offshore Operations.

Horjen, I & Vefsnmo, S 1987, 'Time-dependent sea spray icing on ships and drilling rigs-a theoretical analysis', NHL-report STF60 F.

Jones, KF & Andreas, EL 2009, 'Sea spray icing of drilling and production platforms', Engineer Research and Development Center Hanover NH Cold Regions Research and Engineering Lab.

Jones, KF & Andreas, EL 2012, 'Sea spray concentrations and the icing of fixed offshore structures', *Royal Meteorological Society*, vol 138, pp. 131-144.

Jørgensen, TS 1984, 'Sjøsprøytmålinger på boreriggen "Tresure Scout" - Resultater fra forsøk april 1983 - februar 1984', Norges Hydrodynamiske Laboratorier.

Kulyakhtin, A & Tsarau, A 2014, 'A time-dependent model of marine icing with application of computational fluid dynamics', *Cold regions science and technology*, vol 104, pp. 33-44.

Li, M, Jiang, Y & Coimbra, CFM 2017, 'On the determination of atmospheric longwave irradiance under all-sky conditions', *Solar Energy*, vol 144, pp. 40-48.

Lundqvist, J-E & Uding, I 1977, 'Ice accretion on ships with special emphasis on Baltic conditions', Styrelsen för vintersjöfartsforskning.

Makkonen, L 2010, 'Solid fraction in dendritic solidification of a liquid', *Applied Physics Letters*, vol 96, no. 9, p. 091910.

Maykut, GA & Church, PE 1973, 'Radiation climate of Barrow, Alaska, 1962-66', *Journal of Applied Meteorology*, vol 12, pp. 620-628.

Mertins, HO 1968, 'Icing on fishing vessels due to spray', *Marine Observer*, vol 38, no. 221, pp. 128-130.

Mitten, P 1994, 'Measurement and modelling of spray icing on offshore structures', *Contract no. 07SE. KM169-8-7439, Final Report to Atmospheric Environment Service of Canada*.

Nauman, JW 1984, 'Superstructure Icing Observations on the Semisubmersible Ocean Bounty in Lower Cook Inlet, Alaska', *Second International Workshop on Atmospheric Icing of Structures*, Trondheim.

Overland, JE 1990, 'Prediction of vessel icing for near-freezing sea temperatures', *Weather and forecasting*, vol 5, no. 1, pp. 62-77.

Overland, JE, Pease, CH & Preisendorfer, RW,CAL 1986, 'Prediction of vessel icing', *Journal of climate and applied meteorology*, vol 25, no. 12, pp. 1793-1806.

Sawada, T 1962, 'Icing on ships and its forecasting', *Journal of Japanese Society of Snow and Ice*, vol 24, pp. 12-14.

Shellard, H 1974, 'The meteorological aspects of ice accretion', *Secretariat of the World Meteorological Organization*.

Stallabrass, J 1980, 'Trawler icing: A compilation of work done at NRC', National Research Council of Canada.